Materials Research.
DOI: http://dx.doi.org/10.1590/1980-5373-MR-2017-0930

Morphology and Phase Formation During the Solidification of Al-Cu-Si and Al-Ag-Cu Ternary Eutectic Systems

Carina Morando[a,b,c], Osvaldo Fornaro[a,b,c]*

[a]*Instituto de Física de Materiales Tandil - IFIMAT, Universidad Nacional del Centro de la Provincia de Buenos Aires - UNCPBA, Buenos Aires, Argentina*
[b]*Centro de Investigaciones en Física e Ingeniería del Centro de la Provincia de Buenos Aires – CIFICEN, Universidad Nacional del Centro de la Provincia de Buenos Aires - UNCPBA, Pinto 399, B7000GHG Tandil, Argentina*
[c]*Consejo Nacional de Investigaciones Científicas y Técnicas – CONICET, Godoy Cruz 2290, C1425FQB Buenos Aires, Argentina*

Received: October 12, 2017; Revised: December 20, 2017; Accepted: January 18, 2018

The microstructure of ternary alloys in the Al rich corner of the Al-Cu-Si and Al-Ag-Cu systems were analyzed in order to determine the solidification path in the different structural regions expected from the equilibrium phase diagram. The analysis was based on theoretical models developed in the literature for solidification of ternary eutectic system alloys under simple lever rule assumptions. Optical microscopy (OM), scanning electron microscopy (SEM) and energy dispersive X-ray microanalysis (EDAX) were used to study the microstructure formed in each case. The observations were consistent with model predictions: Al-Cu-Si system showed two binary eutectics: non faceted-non faceted (nf-nf) AlCu and faceted-non faceted (f-nf) AlSi, Al-Ag-Cu system showed 2 binary regular eutectics (nf-nf) and a ternary semi-regular Brick type eutectic. The results provided an example of a methodology for use in ternary and multicomponent alloys.

Keywords: *ternary eutectic systems, solidification structures, Al-Cu-Si/Al-Ag-Cu alloys.*

1. Introduction

Primary manufacturing processes such as ingot casting, continuous casting, squeeze and pressure casting and secondary manufacturing processes such as welding and soldering, involve solidification as an important stage of the process[1]. Many commercial materials are multicomponent alloys, whose mechanical or functional properties are determined by the microstructure that develops during the solidification and subsequent processing stages. One of the essential challenges to materials science is to understand how solidification microstructures form and how they can be controlled by selecting the alloy composition and processing parameters. Thus, a detailed understanding of microstructure formation is important in turn to dictate the performance of the final product[2].

Fundamental knowledge on solidification has been developed mainly for pure materials and for binary alloys exhibiting single phase growth (solid solution) and/or two phase growth in eutectic and peritectic class reactions[3].

The classical analytical description for steady-state eutectic growth in binary alloys, developed by Jackson and Hunt[3], describes the relationship among the undercooling ΔT in front of the isothermal interface, the growth velocity V and the lamellar spacing λ in the case of regular (i.e non faceted-non faceted) growth at low velocity for phases with similar densities:

$$\Delta T = k_1 \lambda V + \frac{k_2}{\lambda} \quad (1)$$

where k_1 and k_2 are constants which depends on the alloy.

It was demonstrated that a two-phase structure tends to form a lamellar structure when the volume fraction of the minor phase has a volume fraction greater than 0.28, whilst for volume fractions less than 0.28 a rodlike morphology has the minimum interfacial energy[4]. This is because an increase in volume fraction for a lamellar structure only increases the relative thickness of one phase in the structure without a change in surface area, while the surface area increases with an increase in volume fraction in a rod type structure. It appears that the morphological nature of a binary eutectic system can be predicted from knowledge of the relative volume fraction of phases present at the eutectic composition, and this can be obtained from the phase diagram using the reverse lever law.

McCartney et al.[5] already gave an onset for extending the Jackson and Hunt´s theory for binary alloys to univariant two-phase coupled eutectic growth as part of the description of the different microstructural regions within a ternary eutectic system, yielding to a Jackson and Hunt type of expression.

*e-mail: ofornaro@exa.unicen.edu.ar

While binary alloys have extensively been studied for decades both from theoretical as experimental points of view, for multicomponent alloys with three or more component, the process of microstructure formation during solidification is less understood especially for cases where multiphase reactions occur along the solidification path of the alloy[5,6]. By other side, directional solidification studies have been performed by several authors in ternary alloys to investigate the morphological stability in dilute ternary systems and the nature and dynamic behavior of the patterns forming in coupled growth[7,8].

Ternary eutectic alloys exhibit a much richer variety of microstructures compared to binary ones. Whereas in regular binary eutectics simply fibrous and lamellar arrangements appear, ternary eutectics can show three phases being arranged in fibers, two fibers embedded in a lamella, two lamellae embedded in a matrix, ladder structures of two phases in a matrix, two phases parallel and one phase orthogonal to it, etc[4].

Because ternary eutectics are mixtures of three phases, they necessarily must have a larger number of morphological classes than binary eutectics. The structure depends on three solid-solid and three solid-liquid interfacial energies and two volume fractions. In analogy to the binary case, for equal interfacial energies and a small volume fraction, a rodlike morphology would be expected for a ternary eutectic.

The most systematic work has been performed by McCartney et al.[5,6] describing some of the microstructural regions occurring in ternary eutectic systems by extension of the known analytical expression in binary alloys for stability of the solid/liquid interface and the competitive growth criterion. Considering a simple ternary system and assuming that each of the three primary phases, α, β and γ, grows in a non-faceted fashion, and nucleate easily, a number of different structural regions are then to be expected[5]. The composition ranges of each of these, for a fixed growth velocity and temperature gradient, and schematic growth interfaces predicted are also given[5].

Himemiya and Umeda[9-11] extended Jackson and Hunt's model for simple geometrical arrangements of the three-phase planar invariant coupled growth in a ternary eutectic system. They also extended their method to set up a microstructural selection map in the case of ternary eutectic solidification based upon analytical growth models and concluded that also in ternary eutectics the Jackson-Hunt´s relationships for the spacing as a function of solidification velocity holds. Real ternary eutectics are much more complex and their structure generally fails to be describable by the Himemiya´s approach. In addition to that, extensive works were performed to describe the experimental behavior through the CALPHAD method for both systems[12-17].

In this way, the structure for these systems must be formed by three distinctive phases. In the case of Al-Cu-Si ternary alloys, the structure would be formed by different phase fractions of α-Al rich phase, with few Cu and Si content, the intermetallic θ phase (Al_2Cu) and a Si-rich phase. For Al-Ag-Cu alloys, an α-Al rich phase, containing Cu and Ag in solution, and intermetallic θ and ζ (Ag_2Al) phases are expected.

The purpose of the present work is to characterize the variety of microstructures arising in Al-rich corner of Al-Cu-Si and Al-Ag-Cu alloys during controlled solidification and to classify them taking into account the various possible types of solidification paths corresponding to the different structural regions of phase diagram. The evaluation is proposed in terms of microstructural observation and equilibrium considerations of the ternary phase diagram.

2. Materials and Methods

Al-Cu-Si alloys of eight different compositions and Al-Ag-Cu alloys of five different compositions were prepared in our laboratory by melting a pre-weighted quantity of pure elements (4N) Al, and AlCu, AlSi or AlAg eutectic binary alloys in a SiC crucible coated internally by ceramic protective paint, heated in an electric resistance-type furnace under inert argon gas flow protection, stirred for adequate homogenization and cast in stainless steel molds. The nominal compositions of the alloys are expressed as weight % of solute.

The molten alloys were forced to flow on a rectangular sectioned channel, of dimensions 369x116x39 mm, under depress-casting. A description of the experimental setup and detailed procedures for processing can be found in References[18,19] where this setup was used to determine the fluidity of these alloys. Samples for metallographic examination were sectioned longitudinally from the obtained castings for each alloy. Standard metallographic procedures were followed using SiC grinding papers up to 600μm using water as a lubricant; continued by polishing with diamond paste up to 1/4 μm using alcohol as a lubricant. In order to reveal the microstructure, Al-Cu-Si alloys were electrolytically polished and etched with: 7,5ml HN_3 + 5ml HCl + 2,5ml HFl in H_2O, while Al-Ag-Cu alloys were electrolytically polished with 80cc of 2Butoxietanol+10cc of Glycerol+10cc $HClO_4$ and chemically etched with HF 0,5% in H_2O.

The microstructure was analyzed using optical microscopy (OM), scanning electron microscopy (SEM) and energy dispersive X-ray microanalysis (EDAX). In addition, solidification paths were determined by the presence of different phases from the metallography.

The nominal composition of the alloys used through this work, and the phases expected according to equilibrium considerations are listed in Table 1 and 2. The molar phase fractions were calculated with Thermo-Calc software (release S) with adequate databases[12,13,15,16]. Figure 1 shows Al-rich corner of Al-Cu-Si phase diagram, dashed lines show the univariant binary eutectic Al-Si and Al-Cu reactions. Figure 2 shows Al-rich corner of Al-Ag-Cu phase diagram, dashed lines are univariant Al-Ag and Al-Cu binary eutectic reactions. The alloys used in this work are added in the Figures.

Table 1. Compositions and constituent phases of the used Al-Cu-Si alloys.

Alloy	Composition	Constituent phases/reaction path	Corresp. to eq.
1	Al-33.2%Cu	$(\alpha+\theta)_{BE}$	
2	Al-11.7%Si	$(\alpha+ Si)_{BE}$	
3	Al-27.5%Cu-5.25%Si	$(\alpha+\theta+ Si)_{TE}$	
4	Al-5%Cu-9%Si	$\alpha\rightarrow(\alpha+ Si)_{BE}\rightarrow(\alpha+\theta+ Si)_{TE}$	(2-a)
5	Al-21%Cu-6%Si		
6	Al-5%Cu-12.5%Si	$Si\rightarrow(\alpha+ Si)_{BE}\rightarrow(\alpha+\theta+ Si)_{TE}$	(2-b)
7	Al-21%Cu-2%Si	$\alpha\rightarrow(\alpha+\theta)_{BE}\ \alpha\rightarrow(\alpha+\theta+ Si)_{TE}$	(2-c)
8	Al-21%Cu-4%Si	$\alpha\rightarrow(\alpha+\theta+ Si)_{TE}$	(2-d)

*α-Al, and θ are defined into the text. ** $(\ )_{BE}$ or $(\ )_{TE}$ for binary or ternary eutectic compositions.

Table 2. Compositions and constituent phases of the used Al-Ag-Cu alloys

Alloy	Composition	Constituent phases/reaction path	Corresp. to eq.
9	Al-70%Ag	$(\alpha+\zeta)_{BE}$	
10	Al-32%Ag-20%Cu	$(\alpha+\theta+\zeta)_{TE}$	
11	Al-5%Ag-10%Cu	$\alpha\rightarrow(\alpha+\theta)_{BE}$	(3-a)
12	Al-10%Ag-10%Cu		
13	Al-40%Ag-10%Cu	$\alpha\rightarrow(\alpha+\zeta)_{BE}\rightarrow(\alpha+\theta+\zeta)_{TE}$	(3-b)

*α-Al, θ and ζ are defined into the text. ** $(\ )_{BE}$ or $(\ )_{TE}$ for binary or ternary eutectic compositions.

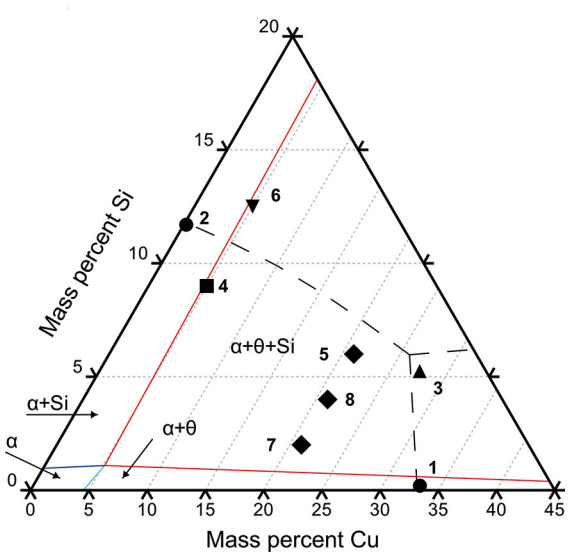

Figure 1. Al-rich corner of Al-Cu-Si phase diagram. Dashed lines show the univariant binary eutectic Al-Si and Al-Cu reactions. The alloys used in this work are added in the graph.

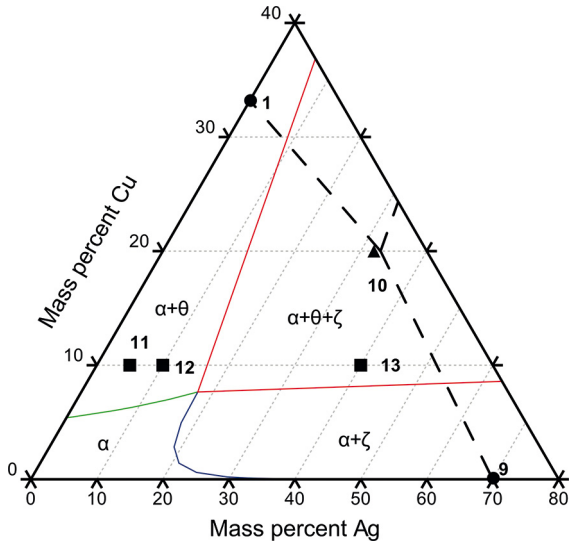

Figure 2. Al-rich corner of Al-Ag-Cu phase diagram Dashed lines are univariant Al-Ag and Al-Cu binary eutectic reactions. The alloys used in this work are added in the graph.

3. Results and Discussion

3.1 Al-Cu-Si ternary eutectic system

The alloys selected for the present work were chosen as representative examples of different structural regions as predicted in the work of McCartney et al.[5,6] for a simple hypothetic ternary eutectic system taking into account the solidification path according to the equilibrium diagram.

Usually, and depending on the volume or constitution of the phase, the primary product of solidification is the coarsest phase visible in the metallography, and could has a dendrite structure in the case of aluminum or faceted crystals for the silicon. The secondary and tertiary structures are successively thinner, due to their lesser molar volume[20]. The expected microstructure for these alloys is formed by a precipitation sequence of a primary phase, followed by a

univariant binary eutectic and a monovariant ternary eutectic reaction. In some cases, the richer liquid falls close to the ternary eutectic composition, and then, the solidification ends in the coupled zone, where a binary reaction could be absent.

Following McCartney et al.[5,6] the results could be represent in different regions or qualitative groups depending on the specific solidification path:

Group I: Binary and ternary eutectics, alloys of two or three phase coupled growth

The typical microstructure of eutectic alloys Al-33.2%Cu, Al-11.7%Si and Al-27.5%Cu-5.25%Si can be seen in Figure 3. The alloy called #1 in Table 1 corresponds to an Al-33.2%Cu binary eutectic alloy. It exhibits a regular lamellar morphology consisting of two non-faceted phases: an α-Al rich phase (white phase in Figure 3 a) and a θ (Al_2Cu) (black phase). The alloy #2 is an Al-11.7%Si binary composition. It presents an irregular eutectic microstructure that consists of a faceted and a non-faceted phase, as shown in Figure 3b). The Si-rich phase present in faceted platelike, grows preferentially into the liquid with a halo of α-Al rich phase. Figure 3c) shows the microstructure corresponding to the eutectic ternary #3 alloy that presents a composition Al-27.5%Cu-5.25%Si. In this case the microstructure is formed by a three-phase's mixture of Silicon (gray in the micrograph), θ (black) in an α-Al matrix (the white area). It can be noticed that the alloys #1, #2 as #3 grow into a coupled binary or ternary composition range.

Group II: Alloys that solidified on the AlSi eutectic valley side

Figure 4 shows typical microstructures of longitudinal sections of a) alloy #4 Al-5%Cu-9%Si, b) alloy #5 Al-21%Cu-6%Si and c) alloy #6 Al-5%Cu-12.5%Si. White, grey and black phases are α-Al, Si and Al_2Cu respectively; interdendritic fine scale phase is ternary eutectic.

As it can be seen in the equilibrium phase diagram of Figure 1, Alloys #4 (Al-5%Cu-9%Si) and #5 (Al-21%Cu-6%Si) follow a solidification path that begins with a primary precipitation of an α-Al phase, whilst the liquid reaches the binary Al-Si eutectic univariant line valley. The composition of alloy #5 is closer than #4 from the ternary composition.

In the micrographs, regions of α-Al rich primary phase dendrites, secondary AlSi present with a complex-regular morphology, and a very fine AlCuSi ternary eutectic structure formed by α + θ + Si. Schematically, the reaction path is represented in the third column of Table 1:

$$\alpha \rightarrow (\alpha + \mathrm{Si})_{\mathrm{BE}} \rightarrow (\alpha + \theta + \mathrm{Si})_{\mathrm{TE}} \qquad (2\text{-a})$$

Figure 5 shows the evolution of the molar phase fraction with the temperature during the cooling of the alloys #4 Al-5%Cu-9%Si, #5 Al-21%Cu-6%Si, the solidification proceed from right to left in the Figure, that is while temperature decreases. As it can be seen, the primary is the α-Al phase, followed by Si which appears as a consequence of the binary reaction, following with θ, which forms part of the ternary reaction. Alloy #5 shows a greater amount of θ phase because its composition is closer to the ternary eutectic composition, which results in a greater molar phase fraction than #4.

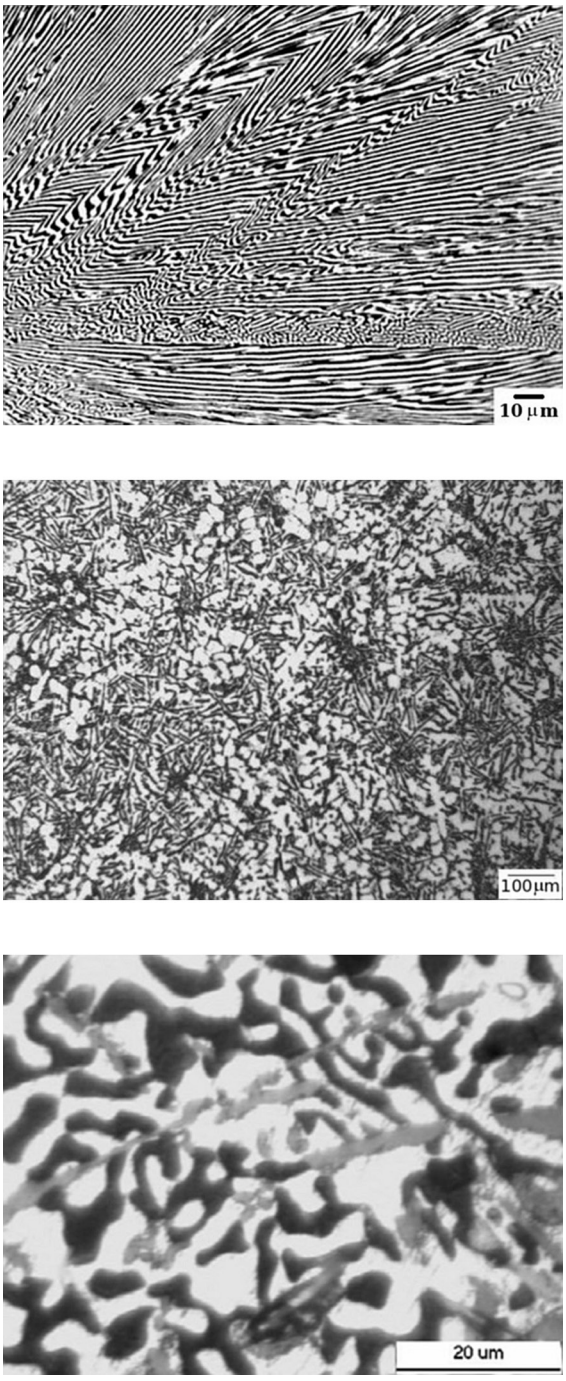

Figure 3. Solidification microstructures corresponding to a) alloy #1 Al-33.2%Cu, b) alloy #2 Al-11.7%Si and c) alloy #3 Al-27.5%Cu-5.25%Si eutectic alloys.

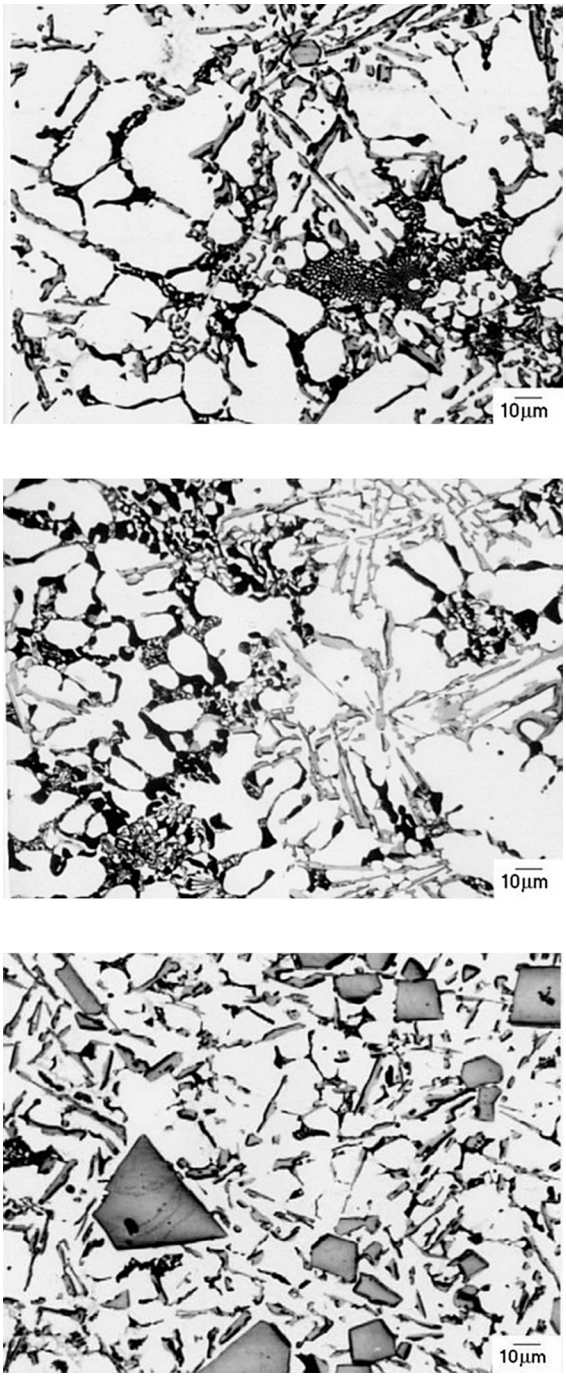

Figure 4. Typical microstructures of longitudinal sections of a) alloy #4 Al-5%Cu-9%Si, b) alloy #5 Al-21%Cu-6%Si; c) alloy #6 Al-5%Cu-12.5%Si; White, grey and black phases are α-Al, Si and Al_2Cu respectively; interdendritic fine scale phase is ternary eutectic.

Alloy #6 (Al-5%Cu-12.5%Si) presents a similar behavior but, in this case, the primary phase is Si randomly distributed and highly faceted, followed by Al-Si binary univariant reaction with acicular microstructure and a monovariant ternary eutectic reaction α + θ + Si of the remnant liquid. The microstructure can be seen in Figure 4 c). During the cooling, this alloy follows schematically a solidification path:

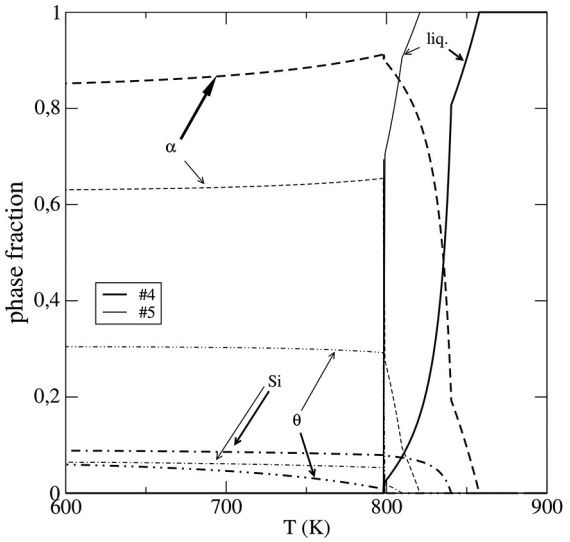

Figure 5. Evolution of molar phase fraction with the temperature during the cooling of the alloys #4 Al-5%Cu-9%Si and #5 Al-21%Cu-6%Si.

$$\mathrm{Si} \rightarrow (\alpha + \mathrm{Si})_{\mathrm{BE}} \rightarrow (\alpha + \theta + \mathrm{Si})_{\mathrm{TE}} \qquad \text{(2-b)}$$

Figure 6 shows the evolution of the molar phase fraction with the temperature during the cooling of this alloy.

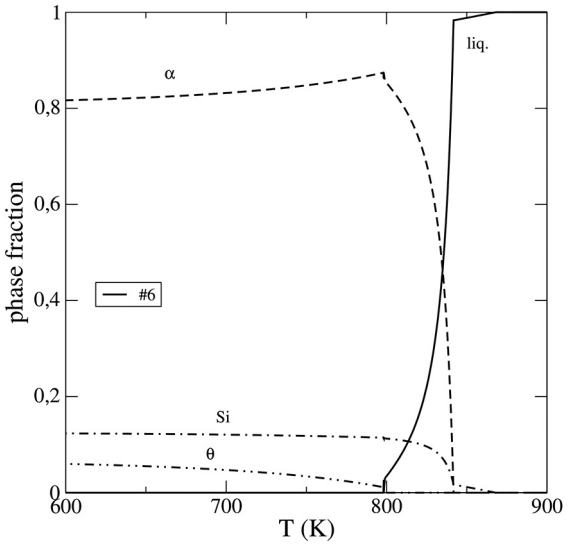

Figure 6. Evolution of molar phase fraction with the temperature during the cooling of the #6 Al-5%Cu-12.5%Si.

Group III: Alloys that solidified on the AlCu eutectic valley side

In the case of the alloy #7 (Al-21%Cu-2%Si), which presents low silicon content, the microstructure revealed the presence of primary α-Al dendrites, followed by secondary binary degenerated eutectic α-Al + θ and fine ternary eutectic, appearing between the dendrite arms, as it is shown in Figure 7. This sequence can be represented as:

$$\alpha \rightarrow (\alpha + \theta)_{BE} \rightarrow (\alpha + \theta + Si)_{TE} \quad (2\text{-c})$$

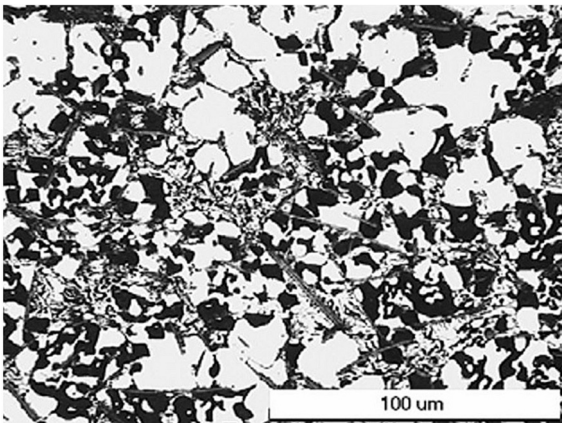

Figure 7. Typical microstructure of longitudinal section of alloy #7 Al-21%Cu-2%Si. White, grey and black phases are α-Al, Si and Al_2Cu respectively; interdendritic fine scale phase is ternary eutectic.

and can be seen in Figure 8.

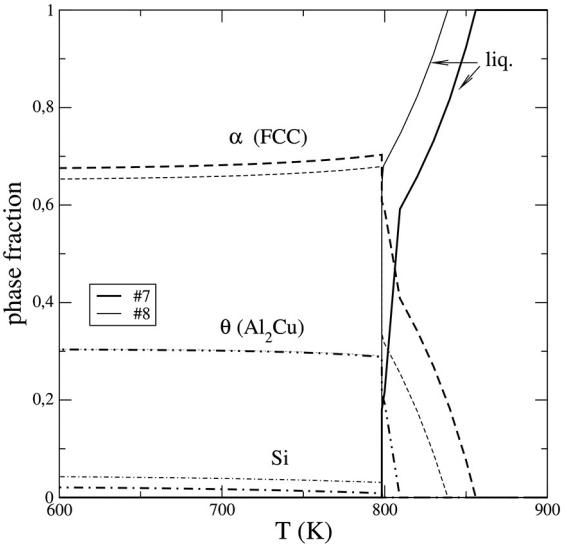

Figure 8. Evolution of molar phase fraction with the temperature during the cooling of alloys #7 Al-21%Cu-2%Si and #8 Al-21%Cu-4%Si.

Group IV: Alloys located on the boundary between the AlCu and Alsi eutectic valleys

Figure 9 shows typical microstructure of longitudinal section of Alloy #8 (Al-21%Cu-4%Si): white, grey and black phases are α-Al, Si and Al_2Cu respectively; interdendritic fine scale phase is ternary eutectic structure. As it can be seen in the image, after the primary phase precipitation, the liquid enriches into the direction of the ternary eutectic composition, or at least falls into the coupled ternary eutectic zone. In this case there is no evidence of binary eutectic transformation during the freezing of this alloy, and then the solidification ends with the ternary eutectic reaction in the form:

$$\alpha \rightarrow (\alpha + \theta + Si)_{TE} \quad (2\text{-d})$$

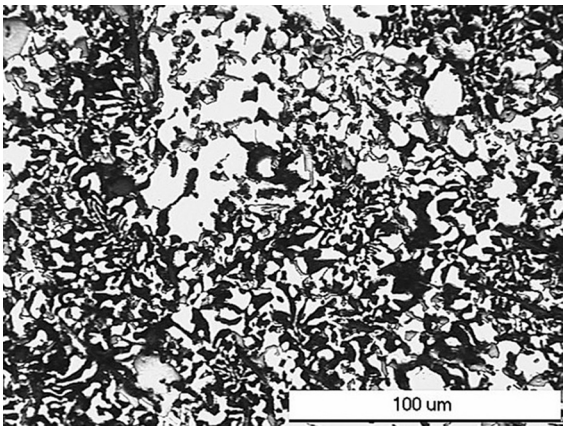

Figure 9. Typical microstructure of longitudinal section of alloy #8 Al-21%Cu-4%Si. White, grey and black phases are α-Al, Si and Al_2Cu respectively; interdendritic fine scale phase is ternary eutectic.

This behavior could be noted in Figure 8 where it can be seen that there isn´t exist formation of molar fraction of θ-phase after the precipitation of α-Al primary phase for the alloy #8, and only appears following the ternary eutectic reaction.

3.2 AlAgCu ternary eutectic system

The alloys selected for this system were chosen as representatives of three different structural regions predicted by McCartney et al.[5,6] in a simple ternary eutectic system within the primary phase area of α-Al. The results are thus divided into three groups as follows:

Group I: Binary and ternary eutectics, alloys of two or three phase coupled growth

Figure 10 shows typical Optical Micrographs (OM) of the microstructure of a) binary eutectic Al-70%Ag (alloy #9) and b) ternary eutectic Al-32%Ag-20%Cu (alloy #10) alloys. Alloy #9 exhibit a regular lamellar morphology, which consists of two non-faceted phases: α-Al rich (clear phase) and ζ (Ag_2Al) (dark phase) and alloy #10 presents a semi-regular or Brick type structure composed by α-Al primary dendrites and two phase dendrites of ζ and θ.

Figure 11 shows typical Scanning Electron Micrographs (SEM) of a) binary eutectic Al-70%Ag (alloy #9) and b) ternary eutectic Al-32%Ag-20%Cu (alloy #10) alloys, where different phases are characterized by energy dispersive X-ray microanalysis (EDAX). In the Figure 11 a), α-Al rich and ζ (Ag_2Al) phases are identified. In Figure 11 b) (Al-32%Ag-20%Cu) α-Al primary dendrites and two phase dendrites of ζ and θ are labeled showed through the EDAX analysis.

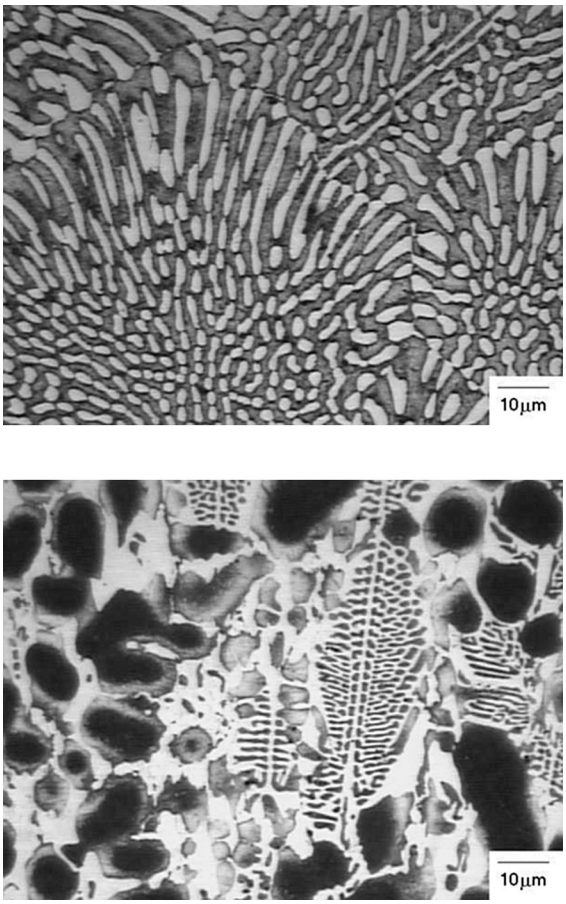

Figure 10. Typical Optical Micrograph (OM) of the microstructure of a) binary eutectic Al-70%Ag (alloy #9) and b) ternary eutectic Al-32%Ag-20%Cu (alloy #10).

Group II: Alloys that solidified on the AlCu eutectic valley side

Figure 12 shows typical Optical Micrographs (OM) of the microstructure of a) Al-5%Ag-10%Cu (alloy #11) and b) Al-10%Ag-10%Cu (alloy #12). Figure 13 show a Scanning Electron Micrograph (SEM) micrograph for Al-10%Ag-10%Cu alloy. The microstructures of these alloys are similar, consisting of α-Al primary phase dendrites (clear phase) and a fine interdendritic phase (dark phase) composed by binary eutectic (α+θ) and ternary eutectic, which can be seen in the micrographs and were determined by EDAX. Under equilibrium considerations, the low silver content should be appearing into the solid solution α-Al and θ phases following a reaction path:

$$\alpha \rightarrow (\alpha + \theta)_{BE} \qquad (3\text{-a})$$

Figure 14 shows the evolution of the molar phase fraction with the temperature during the cooling of alloys #11 (Al-5%Ag-10%Cu) and #12 (Al-10%Ag-10%Cu), showing that the formation of the third phase containing ζ phase appears as a consequence of solid-solid reaction below the ternary eutectic temperature.

Group III: Alloys that solidified on the AlAg eutectic valley side

Figure 15 shows micrographs of Al-40%Ag-10%Cu (alloy #13) a) Optical (OM) and b) Scanning Electron (SEM) images. This alloy presents in its microstructure primary dendrites α-Al (dark phase), binary degenerated eutectic Al-Ag_2Al (clear phase) and fine ternary eutectic in the interdendritic spaces. The detail of this microstructure is shown in the SEM image of Figure 15 b). α-Al, ζ and θ phases were determined by EDAX analysis.

The solidification path follows a reaction:

$$\alpha \rightarrow (\alpha + \zeta)_{BE} \rightarrow (\alpha + \theta + \zeta)_{TE} \qquad (3\text{-b})$$

Figure 16 shows the evolution of the molar phase fraction with the temperature during the cooling for this alloy.

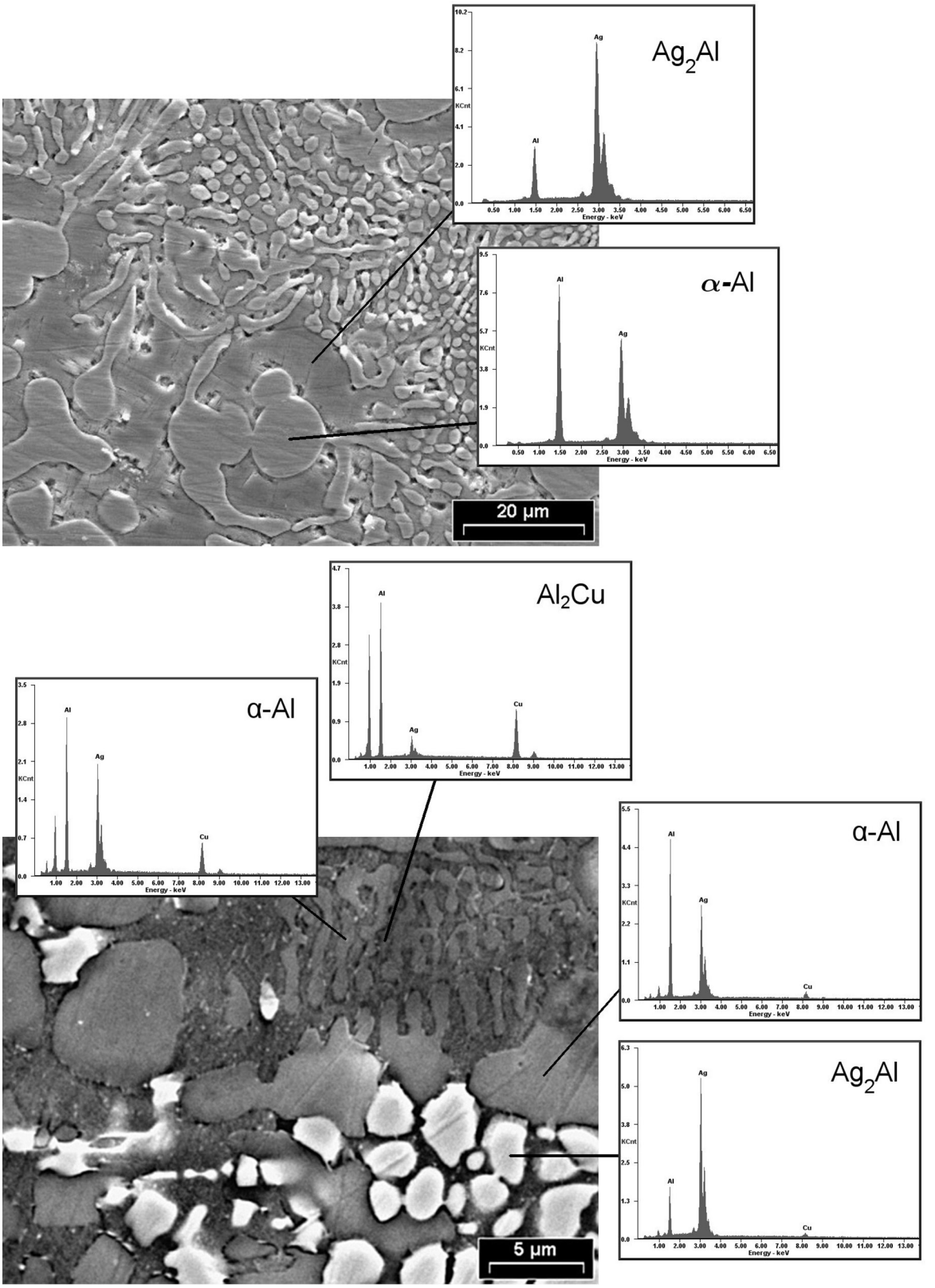

Figure 11. Typical Scanning Electron Micrograph (SEM) of a) binary eutectic Al-70%Ag (alloy #9) and b) ternary eutectic Al-32%Ag-20%Cu (alloy #10).

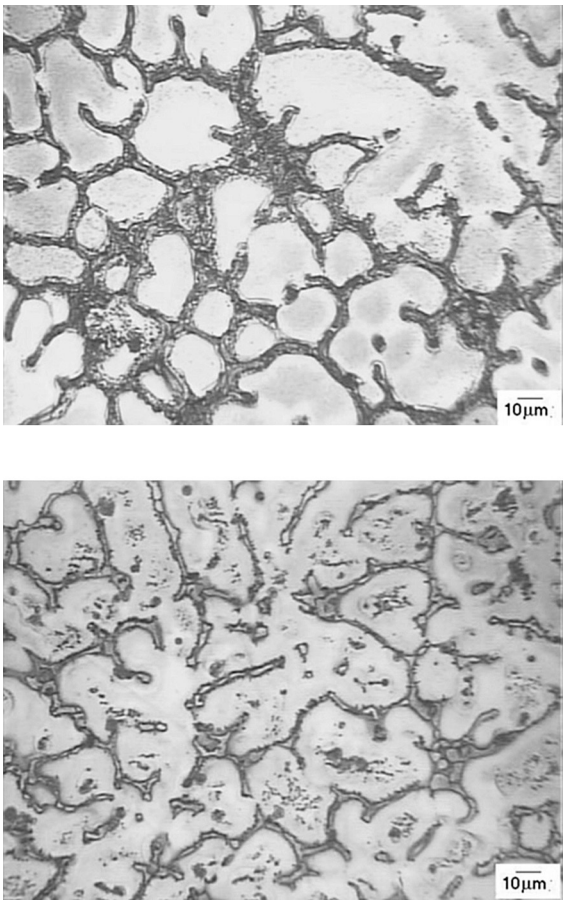

Figure 12. Typical Optical Micrograph (OM) of the microstructure of a) Al-5%Ag-10%Cu (alloy #11) and b) Al-10%Ag-10%Cu (alloy #12).

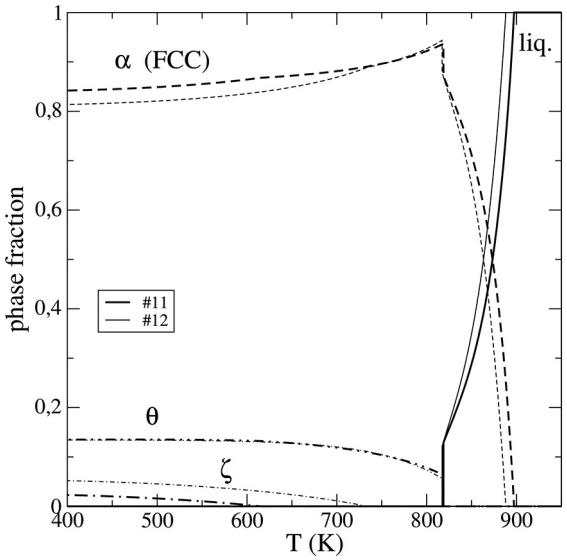

Figure 14. Evolution of molar phase fraction with the temperature during the cooling of alloys #11 (Al-5%Ag-10%Cu) and #12 (Al-10%Ag-10%Cu).

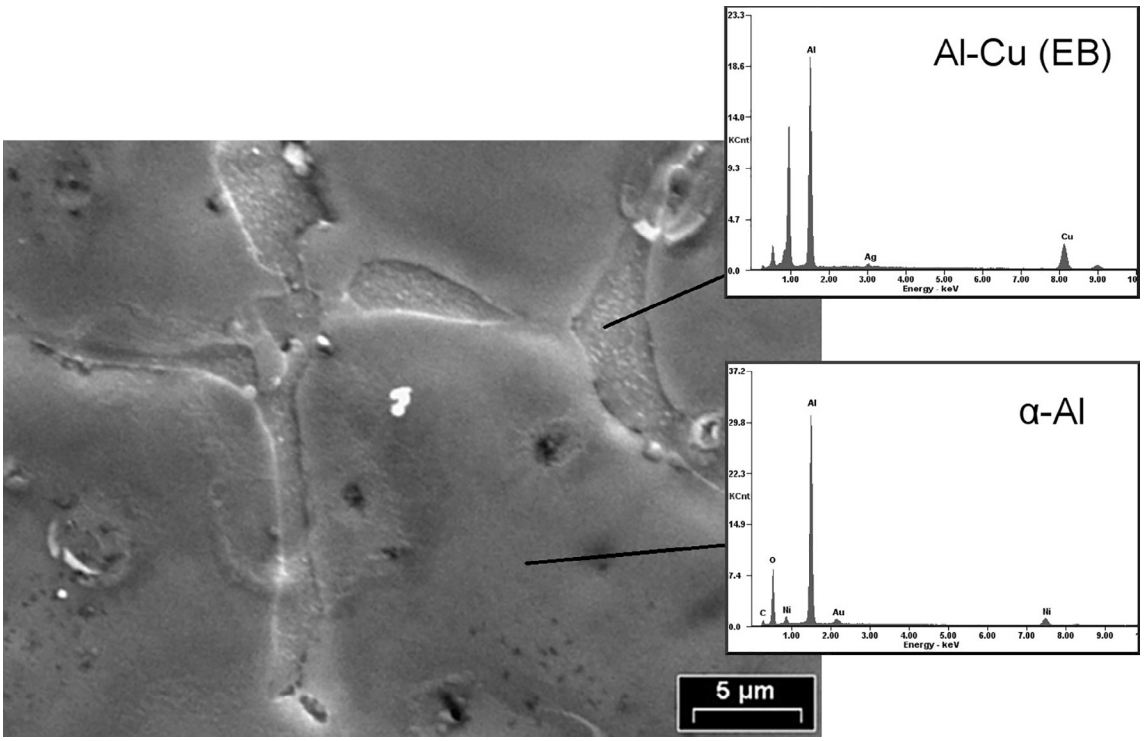

Figure 13. Scanning Electron Micrograph (SEM) of Al-10%Ag-10%Cu (alloy #12).

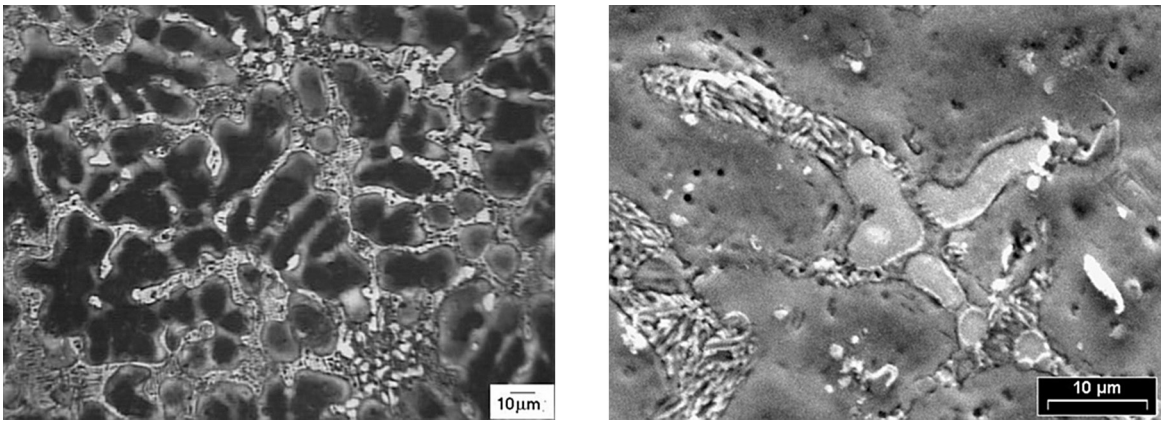

Figure 15. Micrographs of Al-40%Ag-10%Cu (alloy #13) a) Optical Micrograph (OM) and b) Scanning Electron Micrograph (SEM) images.

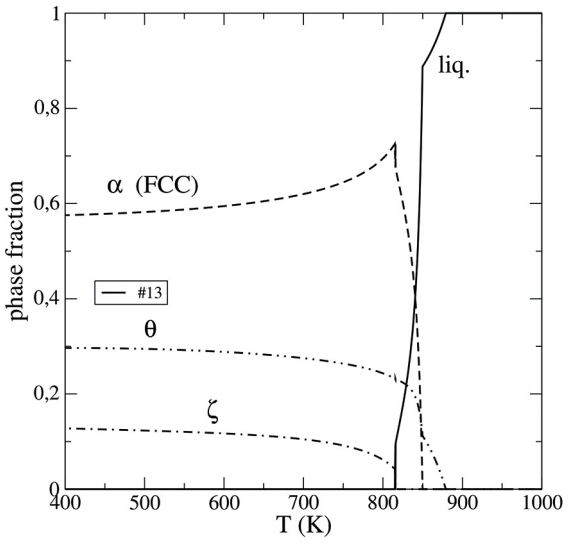

Figure 16. Evolution of molar phase fraction with the temperature during the cooling of alloy #13 (Al-40%Ag-10%Cu).

4. Conclusions

The solidification of eight Al-Cu-Si alloys and five Al-Ag-Cu alloys of different compositions in the Al-rich corner of the phase diagrams, were studied to interpret how the solidification path influence the microstructure formation in these academic ternary systems.

- Generally Al-Cu-Si system shows a combination of non faceted-non faceted AlCu eutectic and faceted-non faceted AlSi eutectic morphologies into a α-Al rich matrix. In this way, theoretical models and phase diagram could be used to predict the existence of different structural regions for each studied composition under the solidification conditions used.
- The Al-Ag-Cu system shows two binary regular eutectic with laminar structures of the non-faceted-non-faceted type, and a ternary eutectic formed by α-Al rich and two-phase dendrites ζ and θ that presents a semi-regular structure of the Brick type.
- This work has showed the existence of several of these structural regions and the types of solidified structures observed were, in general, consistent with the phase sequence formed during solidification according to the lever calculations and model predictions. The results provide an example of an analysis method useful in other ternary or multicomponent alloys such as commercial Al alloys.

5. Acknowledgments

This work was carried out at IFIMAT (UNCPBA-MT) and CIFICEN (UNCPBA-CICPBA-CONICET), and was supported partially by ANPCyT (Agencia Nacional de promoción Científica y Tecnológica), CONICET, SeCAT-UNCPBA (Secretaría de Ciencia, Arte y Tecnología de la UNCPBA).

6. References

1. Phanikumar G, Chattopadhyay K. Solidification microstructure development. *Sadhana*. 2001;26(1-2):25-34.
2. De Wilde J, Nagels E, Lemoisson F, Froyen L. Unconstrained growth along a ternary eutectic solidification path in Al-Cu-Ag: Preparation of a MAXUS sounding rocket experiment. *Materials Science and Engineering: A*. 2005;413-414:514-520.
3. Jackson KA, Hunt JD. Lamellar and Rod Eutectic Growth. *Transactions of Metallurgic Society of AIME*. 1966;226:1129-1142.
4. Lewis D, Allen S, Notis M, Scotch A. Determination of the eutectic structure in the Ag-Cu-Sn system. *Journal of Electronic Materials*. 2002;31(2):161-167.
5. McCartney DG, Hunt JD, Jordan RM. The structures expected in a simple ternary eutectic system: Part 1. Theory. *Metallurgical Transactions A*. 1980;11(8):1243-1249.

6. McCartney DG, Jordan RM, Hunt JD. The structures expected in a simple ternary eutectic system: Part II. The Al-Ag-Cu ternary system. *Metallurgical Transactions A*. 1980;11(8):1251-1257.

7. Boettinger WJ, Coriell SR, Greer AL, Karma A, Kurz W, Rappaz M, et al. Solidification microstructures: recent developments, future directions. *Acta Materialia*. 2000;48(1):43-70.

8. Plapp M, Karma A. Eutectic colony formation: a stability analysis. *Physical Review. E, Statistical Physics, Plasmas, Fluids, and Related Interdisciplinary Topics*. 1999;60(6 Pt B):6865-6889.

9. Himemiya T, Umeda T. Three-Phase Planar Eutectic Growth Models for a Ternary Eutectic System. *Materials Transactions, JIM*. 1999;40(7):665-674.

10. Himemiya T. Growth Models of Two-Phase Eutectic Cell in a Ternary Eutectic System: a Phase Selection Map. *Materials Transactions, JIM*. 1999;40(7):675-684.

11. Himemiya T. Extension of Cellular/Dendritic Eutectic Growth Model to Off-Monovariant Range: Phase Selection Map of a Ternary Eutectic Alloy. *Materials Transactions, JIM*. 2000;41(3):437-443.

12. Dinsdale AT. SGTE data for pure elements. *Calphad*. 1991;15(4):317-425.

13. Saunders N. *COST 507. Thermochemical Database for Light Metal Alloys*. Luxemburg: European Comission; 1998. p. 28-33.

14. Kowalski M, Spencer PJ. Thermodynamic reevaluation of the Cu-Zn system. *Journal of Phase Equilibria*. 1993;14(4):432-438.

15. Witusiewicz VT, Hecht U, Fries SG, Rex S. The Ag-Al-Cu system: Part I: Reassessment of the constituent binaries on the basis of new experimental data. *Journal of Alloys and Compounds*. 2004;385(1-2):133-143.

16. Witusiewicz VT, Hecht U, Fries SG, Rex S. The Ag-Al-Cu system: II. A thermodynamic evaluation of the ternary system. *Journal of Alloys and Compounds*. 2005;387(1-2):217-227.

17. Ponweiser N, Richter KW. New investigation of phase equilibria in the system Al-Cu-Si. *Journal of Alloys and Compounds*. 2012;512(1):252-263.

18. Garbellini O, Palacio HA, Biloni H. Fluidity property vs. Microstructure in binary and ternary alloys at aluminium-rich corner of AlCuSi system. In: *Proceedings of Solidification Processing*. 1987; Sheffield, United Kingdom. p. 327-330.

19. Morando C, Fornaro O, Garbellini O, Palacio HA. Fluidity on Metallic Eutectic Alloys. *Procedia Materials Science*. 2015;8:959-967.

20. Dantzig JA, Rappaz M. *Solidification*. 1st ed. Lausanne: EPFL Press; 2009. 621 p.